BRAIN
ORIGINAL ARTICLE

Riluzole, a glutamate modulator, slows cerebral glucose metabolism decline in patients with Alzheimer's disease

Dawn C. Matthews,[1] Xiangling Mao,[2] Kathleen Dowd,[3] Diamanto Tsakanikas,[3] Caroline S. Jiang,[3] Caroline Meuser,[4] Randolph D. Andrews,[1] Ana S. Lukic,[1] Jihyun Lee,[2] Nicholas Hampilos,[2] Neeva Shafiian,[5,6] Mary Sano,[4] P. David Mozley,[2] Howard Fillit,[7] Bruce S. McEwen,[3,†] Dikoma C. Shungu[2] and Ana C. Pereira[3,5,6,8]

[†]Deceased.

Dysregulation of glutamatergic neural circuits has been implicated in a cycle of toxicity, believed among the neurobiological underpinning of Alzheimer's disease. Previously, we reported preclinical evidence that the glutamate modulator riluzole, which is FDA approved for the treatment of amyotrophic lateral sclerosis, has potential benefits on cognition, structural and molecular markers of ageing and Alzheimer's disease. The objective of this study was to evaluate in a pilot clinical trial, using neuroimaging biomarkers, the potential efficacy and safety of riluzole in patients with Alzheimer's disease as compared to placebo.

A 6-month phase 2 double-blind, randomized, placebo-controlled study was conducted at two sites. Participants consisted of males and females, 50 to 95 years of age, with a clinical diagnosis of probable Alzheimer's disease, and Mini-Mental State Examination between 19 and 27. Ninety-four participants were screened, 50 participants who met inclusion criteria were randomly assigned to receive 50 mg riluzole ($n = 26$) or placebo ($n = 24$) twice a day. Twenty-two riluzole-treated and 20 placebo participants completed the study. Primary end points were baseline to 6 months changes in (i) cerebral glucose metabolism as measured with fluorodeoxyglucose-PET in prespecified regions of interest (hippocampus, posterior cingulate, precuneus, lateral temporal, inferior parietal, frontal); and (ii) changes in posterior cingulate levels of the neuronal viability marker *N*-acetylaspartate as measured with *in vivo* proton magnetic resonance spectroscopy. Secondary outcome measures were neuropsychological testing for correlation with neuroimaging biomarkers and *in vivo* measures of glutamate in posterior cingulate measured with magnetic resonance spectroscopy as a potential marker of target engagement.

Measures of cerebral glucose metabolism, a well-established Alzheimer's disease biomarker and predictor of disease progression, declined significantly less in several prespecified regions of interest with the most robust effect in posterior cingulate, and effects in precuneus, lateral temporal, right hippocampus and frontal cortex in riluzole-treated participants in comparison to the placebo group. No group effect was found in measures of *N*-acetylaspartate levels. A positive correlation was observed between cognitive measures and regional cerebral glucose metabolism. A group × visit interaction was observed in glutamate levels in posterior cingulate, potentially suggesting engagement of glutamatergic system by riluzole. *In vivo* glutamate levels positively correlated with cognitive performance.

These findings support our main primary hypothesis that cerebral glucose metabolism would be better preserved in the riluzole-treated group than in the placebo group and provide a rationale for more powered, longer duration studies of riluzole as a potential intervention for Alzheimer's disease.

Received December 31, 2020. Revised April 07, 2021. Accepted May 22, 2021. Advance access publication June 18, 2021

1 ADM Diagnostics Inc., Northbrook, IL 60062, USA
2 Department of Radiology, Weill Cornell Medicine, New York, NY 10021, USA
3 The Rockefeller University, New York, NY 10065, USA
4 Department of Psychiatry, Alzheimer's Disease Research Center, Icahn School of Medicine at Mount Sinai, New York, NY 10029, USA
5 Department of Neurology, Friedman Brain Institute, Icahn School of Medicine at Mount Sinai, New York, NY 10029, USA
6 Nash Family Department of Neuroscience, Friedman Brain Institute, Icahn School of Medicine at Mount Sinai, New York, NY 10029, USA
7 Alzheimer's Drug Discovery Foundation, New York, NY 10019, USA
8 Ronald M. Loeb Center for Alzheimer's Disease, Icahn School of Medicine at Mount Sinai, New York, NY, 10029, USA

Correspondence to: Ana C. Pereira
Department of Neurology, Icahn School of Medicine at Mount Sinai
1468 Madison Avenue, New York, NY 10029, USA
E-mail: ana.pereira@mssm.edu

Keywords: Alzheimer's disease; riluzole; cerebral brain metabolism; FDG PET; glutamate

Abbreviations: ADAS-Cog = Alzheimer's Disease Assessment Scale-Cognitive Subscale; MMSE = Mini-Mental State Examination; MRS = magnetic resonance spectroscopy; NAA = *N*-acetylaspartate; NPI = Neuropsychiatric Inventory; P C = posterior cingulate; SUVR = standardized uptake value ratio; tCr = total creatinine; W = unsuppressed water signal

Introduction

Alzheimer's disease is the most common neurodegenerative disorder, affecting over 43 million people worldwide with an enormous psychosocial and economic impact on society.[1] Without effective therapies and given a high rate of clinical trial failures, an urgent need remains to identify treatment strategies that can slow progression of Alzheimer's disease neurodegeneration. In this exploratory clinical trial, we evaluated the potential of riluzole, a glutamate modulator that exhibits neuroprotective properties and is approved for amyotrophic lateral sclerosis (ALS), to provide benefit in Alzheimer's disease.

Glutamatergic pyramidal neurons that furnish corticocortical connections between association cortical areas and the excitatory hippocampal connections that subserve memory and cognition are the most vulnerable to damage and loss in Alzheimer's disease.[2,3] The entorhinal cortex, an early site of tau accumulation, consists primarily of pyramidal cells that use glutamate as an excitatory neurotransmitter.[4] The hippocampal and neocortical atrophy characteristic of Alzheimer's disease progression demonstrate degeneration predominantly in large glutamatergic pyramidal neurons.[3,5,6] Glutamate-mediated toxicity has been implicated as one potential mechanism of neuronal loss in Alzheimer's disease.[7] Glutamate overflow to extrasynaptic space and activation of extrasynaptic *N*-methyl-D-aspartate (NMDA) receptors has been hypothesized to allow excessive sodium and calcium influx, degrading mitochondrial function and leading to apoptosis.[8] We have previously shown that downregulation of the major glutamate transporter EAAT2 (or GLT-1) accelerates age-related cognitive decline, and conditional heterozygous astrocytic EAAT2 knockout mice have dysregulated immune signalling that correlated with cognitive performance.[9] The neuropathophysiological hallmarks of Alzheimer's disease, amyloid-β plaques and neurofibrillary tangles formed of hyperphosphorylated tau, have been implicated in glutamatergic dysfunction. Neurofibrillary tangles tend to preferentially accumulate in excitatory pyramidal neurons.[10–12] Tau gene expression and phosphorylation are increased in the setting of glutamate toxicity[13,14] and tau release and propagation through interconnected neural circuits are dependent on neuronal activity.[15–17] Oligomers of amyloid-β disrupt glutamate transporters,[18] leading to spillover and activation of extrasynaptic NMDA receptors, implicated in glutamate-mediated toxicity and inhibition of long term potentiation.[19] Amyloid-β release is dependent on neuronal activity[20] and decreases surface expression of synaptic NMDA receptors,[21] critical for physiological neurotransmission. Glutamatergic dysregulation thus forms a cycle of toxicity in Alzheimer's disease. We have proposed that pharmacological modulation of glutamatergic neural circuits in Alzheimer's disease could diminish toxicity through one or more of these pathways, with the potential to preserve or increase neuronal function. Particularly relevant would be the protection of the pyramidal neurons that are most vulnerable in Alzheimer's disease, through reduced glutamate overflow to extrasynaptic space, reducing glutamate-mediated toxicity and potentially allowing increased synaptic activity.

Our group has previously shown that riluzole can prevent age-related cognitive decline in rodents through clustering of dendritic spines,[22] strengthening neural communication.[23,24] Furthermore, we have shown that riluzole rescues gene expression profiles related to ageing and Alzheimer's disease, and that the most affected pathways were related to neurotransmission and neuroplasticity.[25] More recently, we have demonstrated that riluzole prevented hippocampal-dependent spatial memory decline in an early-onset aggressive mouse model of Alzheimer's disease (5XFAD), reduced amyloid pathology and reversed many of the gene expression changes in immune pathways.[26] These reversals involved microglia-related genes [26] thought to be critical mediators of Alzheimer's disease pathophysiology,[27–29] including a recently identified unique population of disease-associated microglia.[30] Riluzole has also been reported to reduce total tau,[31] which in

clinical studies correlates with glucose metabolism and cognition.[32] Riluzole has been demonstrated to modulate ion channels,[33,34] and to increase neurotrophic factors.[35,36]

Previous research suggests that riluzole-related improvements in astrocytic function and glutamate uptake may produce changes detectable with fluorodeoxyglucose (FDG) PET measurement of glucose metabolism and with magnetic resonance spectroscopy (^{1}H MRS).[37] This may occur through increased activity of the main glutamate transporter in the brain, EAAT2 and glutamate uptake.[31,38–40] In rodent models, riluzole increases glutamate uptake by astrocytes and mitigates astrocytic dysfunction.[38] A tight coupling between glutamatergic activity and cerebral glucose metabolism with stoichiometry close to 1:1 has been demonstrated.[41] Glutamatergic transmission accounts for more than 80% of ATP generated from brain metabolism.[42] In one pathway, astrocytic uptake of glutamate released by neuronal synaptic activity leads to conversion of glucose to lactate by the astrocyte, which is transported to neurons and converted to pyruvate for ATP production.[43] Direct metabolism of glucose by neurons has been described and likewise supports the 1:1 relationship between increases in the glutamate–glutamine cycle and neuronal glucose oxidation.[44] In a ^{1}H-^{13}C MRS study conducted in rats, riluzole administration increased glutamate-C4, GABA-C2 and glutamine-C4 in hippocampus and prefrontal cortex, demonstrating increased glucose oxidative metabolism and glutamate/glutamine cycling between neurons and astroglia.[37]

In the current study, we aimed to translate preclinical findings to human Alzheimer's disease through a pilot phase 2 randomized, double-blind, placebo-controlled clinical trial of riluzole in patients with a diagnosis of mild Alzheimer's disease. We tested the hypotheses that (i) riluzole would mitigate the decline of regional cerebral glucose metabolism in Alzheimer's disease as measured with FDG-PET, a well-established biomarker in Alzheimer's disease; (ii) FDG-PET metabolic brain maps would correlate with cognitive measures; and (iii) riluzole would alter the neuronal viability marker, N-acetylaspartate (NAA), and glutamate levels as a marker of target engagement, both measured with ^{1}H MRS.

Materials and methods

Study design and participants

Patients with a clinical diagnosis of probable Alzheimer's disease based on neurological and neuropsychological evaluation (National Institute on Ageing-Alzheimer's Disease Association, NINCDS-ADRDA criteria),[45,46] Mini-Mental State Examination (MMSE) score of 19 to 27, and 50 to 95 years were enrolled in this pilot phase 2 double-blind, randomized, placebo-controlled study. For inclusion, FDG-PET baseline scans were also evaluated to confirm a lack of a frontotemporal dementia or Lewy body disease pattern of hypometabolism. All participants were stable on acetylcholinesterase (AChE) inhibitors for at least 2 months before starting the trial and continued to take AChE throughout the study with the exception of one participant who had never been on AChE therapy. The study was conducted at two sites (Rockefeller University Hospital and Icahn School of Medicine at Mount Sinai, both in New York City), with the approval of the Institutional Review Boards (IRB) of both Institutions. All neuroimaging was performed at Citigroup Biomedical Imaging at Weill Cornell Medicine under an IRB protocol separately approved by that Institution. Memantine, which acts on the glutamatergic system through a different mechanism than riluzole, was not allowed for 6 weeks before study entrance nor over the study duration. Other exclusion criteria were: abnormal liver function [>2 times the upper limit of normal for alanine aminotransferase (ALT) or aspartate aminotransferase (AST); or bilirubin >1.5 times the upper limit of normal, positive hepatitis serology (Hep. B antigen+ or Hep. C antibody+)], uncontrolled diabetes mellitus (Hba1c > 7), chronically uncontrolled hypertension, MRI contraindication, history of brain disease, current smoker or user of nicotine-containing products, currently taking medications with evidence of glutamatergic activity or effects on brain glutamate levels such as lamotrigine, lithium, opiates, psychostimulants such as amphetamines and methylphenidate, tricyclic antidepressants, benzodiazepines and any other drug that the investigators judged might interfere with the study (participants on those medications could be included in the study but without MRS measurements) and others (full criteria at clinicaltrial.gov NCT01703117).

Participants were randomly assigned in a double-blind fashion to receive riluzole at a dose of 50 mg twice a day or placebo for 6 months, with age-matched cohorts of 50–74 and 75–95 years old. Written informed consent was obtained from participants or their legally authorized representative before initiation of study procedures. Data were periodically reviewed by the study Data Safety and Monitoring Board. Two participants had a delay in end point due to the COVID-19 pandemic (see 'Statistical analysis' section).

Randomization and blinding

Random codes were generated by the hospital pharmacy before study initiation, using fixed seed numbers and validated randomization software, and used in sequence. In each of the two age groups, 24 participant numbers were randomized into balanced blocks of either two or four, which were randomly assigned. Study capsule dosage forms (active and placebo) were prepared by pharmacy staff in a blinded manner using over-encapsulation, and opaque (size 3 capsule shells with Lactose NF as an excipient at Rockefeller University Hospital and size 0 capsule shells with microcrystalline cellulose as an excipient at Mount Sinai Hospital). The active drug product contained FDA-approved 50 mg riluzole tablets. For ease of use and compliance, the pharmacy packaged the blinded capsules into medication bottles or organizer trays. Bottles or trays were labelled in a blinded manner, and included patient name, visit and per protocol dosing instructions. Returned trays/bottles were collected by the pharmacy and patient returns, including capsule counts, were recorded by the pharmacy. All encapsulation, packaging and labelling procedures were double verified by pharmacy staff before dispensing.

Procedures

All study personnel had training on study procedures and assessments. A board-certified neurologist made a neurological assessment and administered the MMSE to all participants. FDG-PET scans were acquired at baseline and at 6 months. ^{1}H MRS was performed at baseline, 3 months and 6 months. A neuropsychological testing battery was performed by a licensed neuropsychologist at Rockefeller University and supervised by one at Mount Sinai at baseline, 3 months and 6 months. Patients were seen once a month in clinic for clinical assessment and blood samples were obtained at every visit for safety laboratory exams; blood test results were evaluated by a physician not directly involved in the study to maintain physician-investigators blind.

Outcome measures

Primary end points were: (i) change from baseline to 6 months in cerebral glucose metabolism measured with FDG-PET in posterior cingulate cortex, hippocampus, precuneus and medial temporal, lateral temporal, inferior parietal and frontal lobes, referred to

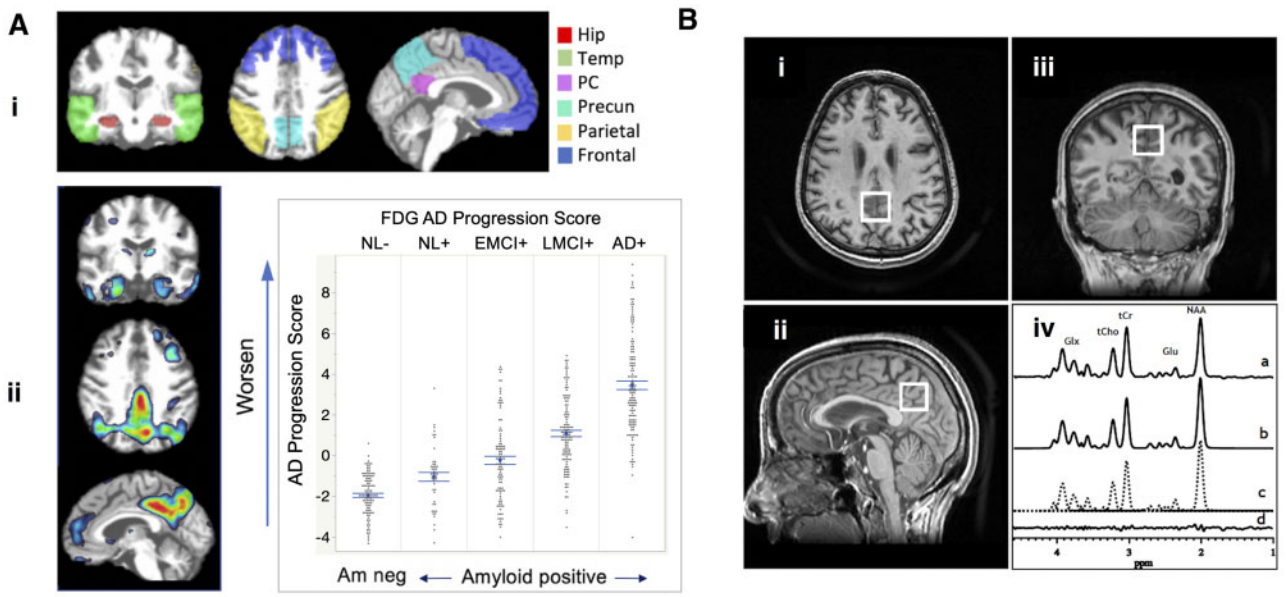

Figure 1 Neuroimaging measures for the study: FDG-PET (*left*) and ^{1}H MRS (*right*). [**A(i)**] Prespecified regions of interest, which were masked with each participant's grey tissue segment. [**A(ii)**] Alzheimer's disease progression classifier pattern, in which increasing progression scores reflect increasing expression of the pattern (subset shown) of hypometabolism (blue) and preservation (red) relative to whole brain. The progression scores of 517 test participants from amyloid negative cognitively normal status through amyloid-positive early mild cognitive impairment (EMCI), late MCI (LMCI) and Alzheimer's dementia (AD) are shown, with mean and standard error, illustrating the correspondence between increased score and worsening clinical severity (data derived using FDG-PET scans from ADNI, www.adni-info.org, as described in Matthews *et al.*[51]). [**B(i)**] Axial, **(ii)** sagittal and **(iii)** coronal magnetic resonance images of a human brain, with depiction of the size and placement of the voxel of interest in the posterior cingulate cortex (PC). PC voxel dimensions: 2.0 cm (anterior–posterior) × 2.0 cm (left–right) × 2.0 cm (superior–inferior) or 8 cm^{3}. [**B(iv)**] Sample CT-PRESS MRS data from the PC voxel, showing (**a**) an experimental spectrum with a clearly resolved C-4 glutamate (Glu) resonance at 2.35 ppm, as well as the resonances for NAA, total creatine (tCr), total choline (tCho) and combined resonances of C-2 glutamate and C-2 glutamine (Glx); (**b**) model fitting of spectrum in **a** to obtain the metabolite peak areas of interest; (**c**) individual components of the model-fitted spectrum in **a**; (**d**) residuals of the difference between spectra in **a** and in **b**.

collectively as our prespecified regions of interest; and (ii) changes in ^{1}H MRS measures of NAA in posterior cingulate (PC) at 6 months. Secondary outcome measures were neuropsychological testing [Alzheimer's Disease Assessment Scale-Cognitive Subscale (ADAS-cog[47,48]), Alzheimer's Disease Cooperative Study (ADCS) Activities of Daily Living (ADL Inventory[49]), Neuropsychiatry Inventory (NPI[50]) total and other measures of memory, executive, visuospatial, attention and language functions for correlation with neuroimaging biomarkers. Another secondary outcome measure was *in vivo* measurement of glutamate with ^{1}H MRS in PC as a marker of target engagement at 3 and 6 months compared to baseline. ^{1}H MRS measures were obtained in bilateral hippocampi as a predefined exploratory outcome. Each FDG-PET image was also analysed using a previously developed Alzheimer's disease Progression Classifier [Fig. 1A(ii)] that quantifies the degree to which a pattern of hypometabolism and preservation relative to whole brain is expressed.[51] Increases in classifier score correspond to increased expression of a pattern of hypometabolism that corresponds to the progression of Alzheimer's disease as validated using over 500 ADNI participants.[51]

As *post hoc* exploratory analyses, relationships between the FDG-PET and MRS measures and the cognitive end points were examined. NPI scores and FDG-PET in the orbitofrontal cortex, a region associated with disinhibition, apathy and other neuropsychiatric attributes,[52,53] were examined for potential association. MRS outcomes in NAA were evaluated at 3 months, and total creatinine (tCr), and other brain metabolites were examined at 3 and 6 months. A composite subregion of posterior cingulate and inferior precuneus was measured on *post hoc* basis to maximize spatial overlap with the boundaries defined in the MRS scans. Subgroup analyses were conducted, stratified by *APOE* ε4 carrier status, age group and sex. Age was of interest due to differences in clinical rates of decline and in the distribution of tau pathology in younger versus older Alzheimer's disease patients.[54]

FDG-PET methods

For each FDG-PET scan, 5 mCi of FDG was administered followed by a 40-min uptake period during which the participant was in a resting state with eyes and ears open, without activity or audiovisual distraction. Images were acquired on a Siemens Biograph 64mCT scanner as a series of four frames of 5 min each. In some initial cases, a full dynamic scan was performed and late timeframes were extracted for processing and analysis.

All PET images were inspected for motion or artefact. Using SPM12 (Wellcome Trust), motion correction was performed and frames averaged into a static image. Each 6-month scan was co-registered to the baseline FDG scan, which was co-registered to the participant's T_1-weighted MRI scan. MRI scans were segmented into grey, white and CSF tissue and spatially transformed to a template in MNI space, and the spatial transformations applied to the PET scans. Regions of interest [Fig. 1A(i)] adapted from Freesurfer[55,56] atlases were thresholded with a smoothed grey participant-specific segment and average intensities within each region of interest were measured. A reference region for calculation of standardized uptake value ratios (SUVRs) was defined based on preserved voxels in the Alzheimer's disease Progression Classifier, most pronounced in the paracentral region. Longitudinal changes in SUVRs using this reference were compared to SUVRs referenced to (separately) centrum semi-ovale white matter, cerebellum, pons and whole brain. While these regions tend to be more variable due to technical factors (cerebellum, pons), progressive hypometabolism effects (whole brain) or potentially affected by

riluzole (cerebellum),[57] consistency in results could help to confirm the robustness of findings. Images were also evaluated (scored) using the FDG Alzheimer's disease Progression Classifier.

MRI and ^{1}H MRS methods

All MRS neuroimaging studies were conducted on a multinuclear 3.0 T GE SIGNA HDx or Discovery MR750 system. Each enrolled participant underwent high resolution axial T_1-, T_2- and spin density-weighted scans. These images were used to prescribe the voxels of interest for the ^{1}H MRS scans. A T_1-weighted volumetric scan was acquired using a spoiled gradient-recalled echo sequence (SPGR, repetition time 12.21 ms, echo time 5.18 ms, flip angle = 7°, voxels 0.94 × 0.94 × 1.5 mm) on the GE HDx system or a magnetization-prepared rapid gradient-echo sequence (MPRAGE, repetition time 8.34 ms, echo time 1.7 ms, flip angle = 7°, voxels 0.94 × 0.94 × 1.5 mm) on the GE Discovery MR750, along with an axial fast FLAIR scan for brain tissue segmentation and use in PET image co-registration and region of interest definition, and to rule out exclusionary focal brain lesions.

In vivo brain levels of glutamate, NAA, tCr and other major metabolites were obtained using ^{1}H MRS and a 2 × 2 × 2-cm^3 PC cortex voxel of interest [Fig. 1B(i–iii)], in ∼6.5 min using the constant-time point-resolved spectroscopy (CT-PRESS) technique[58,59] with echo time 30 ms, 129 constant-time increments (t1) of 0.8 ms and repetition time 1500 ms, and a receive-only eight-channel phased-array head coil, as we recently described.[60] The distinguishing feature of CT-PRESS is that it enables MRS measurement of glutamate uncontaminated by glutamine.[58,59] Figure 1B(iv) presents a sample PC CT-PRESS spectrum acquired in 6 min, and its processing to derive the levels of the metabolites of interest.

Methods for ^{1}H MRS of hippocampi obtained for exploratory analysis are in the Supplementary material.

^{1}H MRS data processing and quantification

Using previously described spectral quality assessment criteria,[61] the areas of the individual spectral peaks, which are proportional to their respective concentrations, were obtained by frequency-domain fitting each resonance to a Gauss–Lorentz (i.e. pseudo-Voigt) lineshape function using the Levenberg–Marquardt non-linear least-squares algorithm as implemented in ^{1}H MRS data processing software written in IDL[61] and illustrated in Fig. 1B(iv) and Supplementary Fig. 2A(d) for CT-PRESS and J-edited spectra, respectively. The levels of NAA, glutamate, GABA, Glx and other metabolites were expressed semi-quantitatively as ratios of peak areas relative to that of the unsuppressed water signal (W) from the same voxels, as previously described.[61] For consistency with earlier MRS literature, levels of the same metabolites were also expressed as peak ratios relative to tCr area in the same voxel. To estimate the proportions of grey matter, white matter and CSF contained in the voxels of interest, SPM8 (http://www.fil.ion.ucl.ac.uk/spm) and in-house program in MATLAB (https://www.mathworks.com/products/matlab.html) were used to generate the proportions of grey matter, white matter and CSF for each voxel.

Statistical analysis

Placebo and treatment groups were compared to identify potential baseline differences in region of interest SUVRs and in age, sex, *APOE* ε4 dose and carrier status, and MMSE score. The 6-month change in SUVR in each region of interest was compared across groups using a one-way analysis of covariance model with the change in SUVR value as the dependent variable, study arm as the categorical independent variable, and baseline SUVR value as a continuous variable covariate (JMP v.15, SAS software) (results were consistent with use of post-treatment SUVR as the independent variable). Age, gender, *APOE* ε4 carrier status and baseline MMSE were investigated as covariates. Assumptions including normal distribution, homogeneity of variance and linear correlation between baseline and post-treatment SUVR were verified, and the number of covariates in a given parametric model was limited to 1–3. Non-parametric tests were applied depending on the number of participants per analysis group and other assumption tests. Effect sizes were calculated using Cohen's *d*. For the two participants who received their FDG-PET scan 2 and 3 months after the 6-month time point due to restrictions arising from COVID-19, the change in value was adjusted using a linear proportional reduction (e.g. value × 6/8 or 6/9). Groups were evaluated *post hoc* without these two participants. ^{1}H MRS data, with three time points, were analysed using linear mixed effects models with group, time point and group × time point interaction as fixed effects and participant as a random effect (SAS Studio v.3.8). In this exploratory study, a *P*-value of less than 0.05 was considered significant and correction for multiple comparisons was not prespecified. However, results using a Bonferroni correction for multiple comparisons were also reported for significant primary end points.

Non-prespecified FDG and MRS data were evaluated in the same manner as prespecified outcomes, without correction for multiple comparisons. The study was not statistically powered for clinical end points or these additional MRS measures, but directional trends were examined for potential effect.

Data availability

Anonymized data will be shared by request from a qualified academic investigator for the sole purpose of replicating procedures and results presented in the article and as long as data transfer is in agreement with IRB of the involved Institutions, which should be regulated in a material transfer agreement.

Results

Sample characteristics and demographics

A total of 94 participants were screened at the two performance sites, of which 44 did not meet inclusion/exclusion criteria. The remaining 50 participants were randomly assigned to receive riluzole (n = 26) or placebo (n = 24). Of these, 22 patients receiving riluzole and 20 patients receiving placebo completed the study and had both FDG-PET time points. The diagram in Fig. 2 shows the participant disposition.

Enrolled participants comprised 26 females and 16 males, aged 58 to 88, and 58% were apolipoprotein 4 (*APOE* ε4) carriers (Table 1, one participant unavailable). There were no significant between-group differences in baseline characteristics of the patients with respect to age, sex, education or *APOE* ε4, although there was a trend for a greater proportion of *APOE* ε4 carriers in the riluzole group. Baseline neuropsychological measures were well balanced for MMSE, NPI, ADL total, Clinical Dementia Rating scale total in riluzole group in comparison to placebo; however, the riluzole group trended as more impaired in ADAS-cog than placebo at baseline (P = 0.08; Table 1).

Neuroimaging outcome measures

FDG-PET

The study's main primary outcome measure confirmed a difference between arms in FDG-PET cerebral metabolic changes over the 6-month treatment period, with less decline in multiple

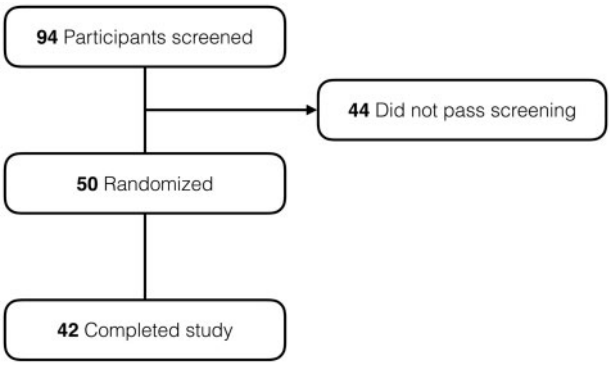

Figure 2 Enrolment, randomization and trial completion.

prespecified brain regions in the riluzole group in comparison to placebo group.

There were no significant or trend-level differences between study arms at baseline in the regional SUVRs that were compared, or in the FDG Alzheimer's disease progression score. Given the trend-level difference between study arms in *APOE* ε4 dose, analyses were performed and compared with and without its inclusion as a covariate. Supplementary Table 3 presents the mean, standard deviation and significance findings for the FDG-PET comparisons. PC glucose metabolism, a primary end point, was significantly preserved in the riluzole-treated group in comparison to placebo over the 6-month period [effect size (*d*) 1.31; $P < 0.0002$] with *APOE* ε4 dose included as covariate, $P < 0.0003$ without *APOE* ε4 dose included, with the effect significant using any of several different reference regions (paracentral $P < 0.0002$, centrum ovale $P < 0.008$, whole brain $P < 0.016$, cerebellar cortex $P < 0.03$) (Fig. 3A–C). PC significance readily survived Bonferroni correction for multiple comparisons. Regional cerebral glucose metabolism was more preserved in the riluzole group in comparison to placebo in several other prespecified regions of interest including precuneus ($P < 0.007$, $d = 0.84$), lateral temporal ($P < 0.014$, $d = 0.80$), right hippocampus ($P < 0.025$, $d = 0.72$) and frontal cortex ($P < 0.035$, $d = 0.67$), and the exploratory subregions of orbitofrontal cortex ($P < 0.008$, $d = 0.86$) and PC-precuneus subregion ($P < 0.007$, $d = 0.88$) (Fig. 4). Most of these still showed trend-level significance if corrected for multiple comparisons. Age, sex, education and *APOE* ε4 dose were not significant contributors to treatment effect. No differences were observed in control regions such as subcortical white matter, pons and cerebellar vermis.

When groups were stratified and analysed separately on a *post hoc* basis (using non-parametric tests due to subgroup size) by *APOE* ε4 carrier status, age and sex, the treatment effect of riluzole group having less decline than placebo was observed in both *APOE* ε4 carriers and non-carriers [$P < 0.004$ in carriers ($n = 8$ placebo, 15 riluzole, effect size 1.526) and $P < 0.09$ in non-carriers ($n = 11$ placebo, 7 riluzole, $d = 0.89$), in both younger and older groups ($P < 0.002$ in older group, $n = 13$ placebo, 15 riluzole, $d = 1.370$ and $P < 0.08$ in younger group, $n = 7$ placebo and seven riluzole, $d = 0.96$); Fig. 3D], and in males and females (both groups $P < 0.02$; $n = 14$ placebo, 12 riluzole in female group and $n = 6$ placebo, 10 riluzole in the male group). Inclusion of *APOE* ε4 dose in the by-age group analysis increased the *P*-value for study arm to 0.13 in the younger group, with *APOE* ε4 dose showing a trend-level influence in this age group ($P < 0.07$) but not the older age group ($P < 0.78$). Inclusion of *APOE* ε4 dose in the by-sex group analysis decreased the *P*-value for study arm to $P < 0.008$ in the female group, with *APOE* ε4 dose showing a trend-level influence in the female group ($P < 0.09$) but not the male group ($P < 0.84$).

Table 1 Demographic and baseline clinical characteristics

Characteristic	Placebo ($n = 20$)	Riluzole ($n = 22$)	*P*-value
Age, years, mean SD	74.6 7.7	75.3 5.8	0.73
Sex, *n* (%)			0.30
Female	14 (70.0)	12 (54.5)	
Male	6 (30.0)	10 (45.5)	
Race/ethnicity, *n* (%)			1.00
Black or African American	0 (0)	1 (4.5)	
Black/non-Hispanic	1 (5.0)	0 (0)	
Latino/Hispanic	0 (0)	1 (4.5)	
White/non-Hispanic	19 (95.0)	20 (90.9)	
Education, years, mean SD	15.1 3.1	15.9 3.0	0.39
APOE ε4 carrier, *n* (%)	8 (40.0)	15 (68.2)	0.11
Clinical scales, mean SD			
ADAS-cog	17.9 7.5	22.5 7.9	0.08
ADL total	68.1 9.3	68.4 9.5	0.91
CDR-sum of boxes	3.6 1.8	3.8 1.9	0.73
CDR total	0.6 0.2	0.6 0.2	0.59
MMSE	22.8 2.9	22.5 2.5	0.72
NPI	10.2 11.1	9.6 9.2	0.86
GDS	5.3 3.7	5.2 6.6	0.98

ADL = Activities of Daily Living Inventory scale; CDR = Clinical Dementia Rating scale; GDS = Geriatric Depression Scale.

FDG-PET measures have been shown to correlate with cognitive decline and predict disease progression.[62–64] The exploratory FDG-PET Progression Classifier score analyses showed a trend of less increase (less worsening) in Alzheimer's disease progression score in the riluzole group in comparison to placebo ($P < 0.07$; Fig. 5A). There was a trend-level greater difference between arms in *APOE* ε4 carriers than non-carriers. FDG-PET Alzheimer's disease progression scores correlated with ADAS-cog at baseline (all participants $R = 0.61$, $P < 0.00002$; placebo group $R = 0.57$, $P < 0.008$; riluzole group $R = 0.48$, $P < 0.0004$) and changes in FDG Alzheimer's disease progression scores correlated with changes in ADAS-cog (all participants $R = 0.46$, $P < 0.002$; placebo group $R = 0.56$, $P < 0.011$; riluzole group $R = 0.29$, not significant and reduced range of score increases) (Fig. 5B) over the 6 months of the study. Additional correlations were observed between FDG-PET and cognitive measures as shown in Fig. 6, including relationships between baseline FDG Alzheimer's disease progression score and MMSE ($R = 0.61$, $P < 0.00002$; Fig. 6A), FDG PC SUVR and MMSE ($R = 0.35$, $P < 0.00003$; Fig. 6B), lateral temporal SUVR and ADAS-cog ($R = 0.54$, $P < 0.0002$; Fig. 6C) and orbitofrontal SUVR and NPI score ($R = 0.52$, $P < 0.0004$; Fig. 6D). The robust correlations observed between FDG-PET brain metabolism and cognitive measures in our dataset support our secondary outcome measure related to neuropsychological assessment.

^{1}H MRS

Voxel tissue composition and spectral quality

The proportions of grey matter, white matter or CSF in the PC or the hippocampal voxels did not differ between groups. Except for an inconsequential increase in the full width at half maximum of the PC water resonance between baseline (4.5 Hz) and 6 months (6 Hz), the spectral quality parameters were remarkably stable, with no group differences in the unsuppressed reference tissue water signal (W) or signal-to-noise ratios observed as a function of time in any of the voxels. The voxel tissue composition and

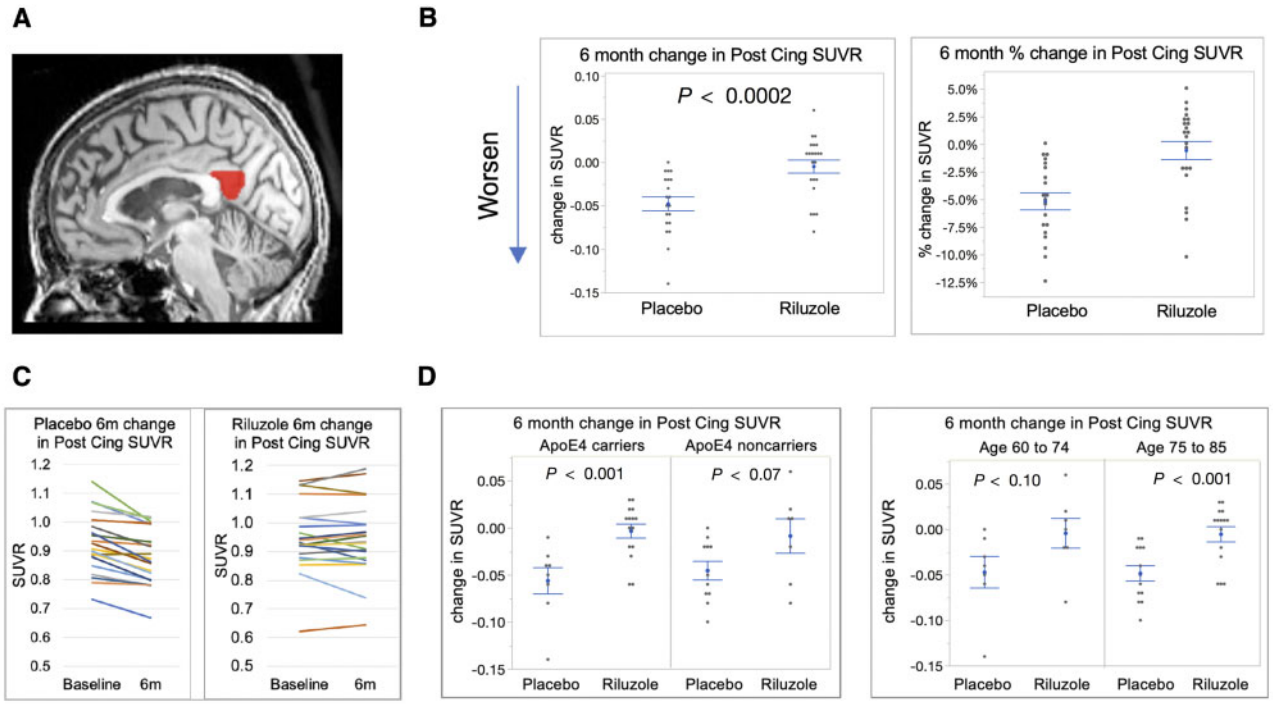

Figure 3 Comparison of changes in FDG-PET in PC over 6 months. (**A**) PC region of interest (representative sagittal slice) in FDG-PET. (**B**) Comparison between placebo and riluzole-treated arms of the absolute and percentage change in PC FDG SUVR over the 6-month treatment period. (**C**) Individual change from baseline to follow up in PC SUVR in placebo (*left*) and riluzole (*right*) treated arms. (**D**) Comparison of change in PC SUVR by *APOE* ε4 carrier and non-carrier subgroups, and by younger and older age groups. Individual values are shown with mean and standard error bars.

spectral quality control data are summarized in Supplementary Table 2.

Posterior cingulate ^{1}H MRS results

As a primary end point, neither NAA/W nor NAA/tCr showed a temporal change (group × visit interaction: $P = 0.14$ or $P = 0.89$, respectively) (Supplementary Fig. 1). ^{1}H MRS results in secondary end point PC glutamate (Glu) levels showed a group × visit interaction when expressed as Glu/tCr ($P = 0.05$) and a trend-level interaction when expressed as Glu/W ($P = 0.3$), with both levels increasing after the first 3 months of treatment (Fig. 7A). No significant changes from baseline to 6 months were observed. In *post hoc* analyses, within the riluzole group NAA/W and Glu/W levels were correlated positively for all three time points, while NAA/tCr and Glu/tCr were positively correlated at baseline (Fig. 7B). Within the placebo group, both NAA/W versus Glu/W and NAA/tCr versus Glu/tCr were positively correlated for all three time points (Fig. 7B).^{1}H MRS measures of Glu/W correlated positively with MMSE and negatively with ADAS-cog across all participants (Fig. 7C). Across all participants Glu/tCr positively correlated with MMSE ($P = 0.01$) but not ADAS-cog ($P = 0.39$).

Hippocampal ^{1}H MRS results

On an exploratory basis, a significant increase in GABA/W was observed in the left hippocampus with a significant group × visit interaction ($P = 0.03$) (Supplementary Fig. 2B) and as a trend level in GABA/tCr ($P = 0.3$). Left hippocampus GABA/W levels positively correlated with memory performance; see Logical Memory 1 and 2 testing correlations at baseline in Supplementary Fig. 2C. No significant changes were seen in any measure of Glx or NAA levels in right or left hippocampus nor GABA levels in right hippocampus.

Neuropsychological testing was a secondary measure for correlation with neuroimaging biomarkers, although the study was not powered for a significant neuropsychological effect. Trend-level findings are shown in Supplementary Fig. 3 for the key functional measures of ADL Inventory, NPI and ADAS-cog.

Adverse events

There were no statistical differences in adverse events between treatment groups, with 23 of 26 patients (88.5%) in the riluzole group and 22 of 24 (91.7%) in the placebo group having at least one adverse event during the study. Serious adverse events occurred in 2 (7.7%) in the riluzole group and 1 (4.2%) in the placebo group. The most common side effects in the riluzole group consisted of abdominal discomfort (15.4% in riluzole, none in placebo); diarrhoea (15.4% in riluzole, 8.3% in placebo); dizziness (15.4% in riluzole, 4.2% in placebo); urinary frequency (11.5% in riluzole and none in placebo), nausea (7.7% in riluzole, none in placebo), cough (19.23% in riluzole, 12.5% in placebo), elevated liver enzymes (7.7% in riluzole and 4.2% in placebo) and others (Supplementary Table 1). Among the randomized patients, 4 of 26 (15.4%) in the riluzole group and 3 of 24 (12.5%) in the placebo group had an adverse event that led to removal from the trial. There were no significant differences in the frequency of participants who were discontinued from the trial due to adverse events.

Discussion

The results of this pilot double-blind, randomized, placebo-controlled trial of riluzole 50 mg twice daily in patients with Alzheimer's disease have confirmed our primary hypotheses, showing 6 months of riluzole treatment to be associated with less decline in FDG-PET measures of cerebral glucose metabolism compared to placebo. The effect was most robust in PC, but effects

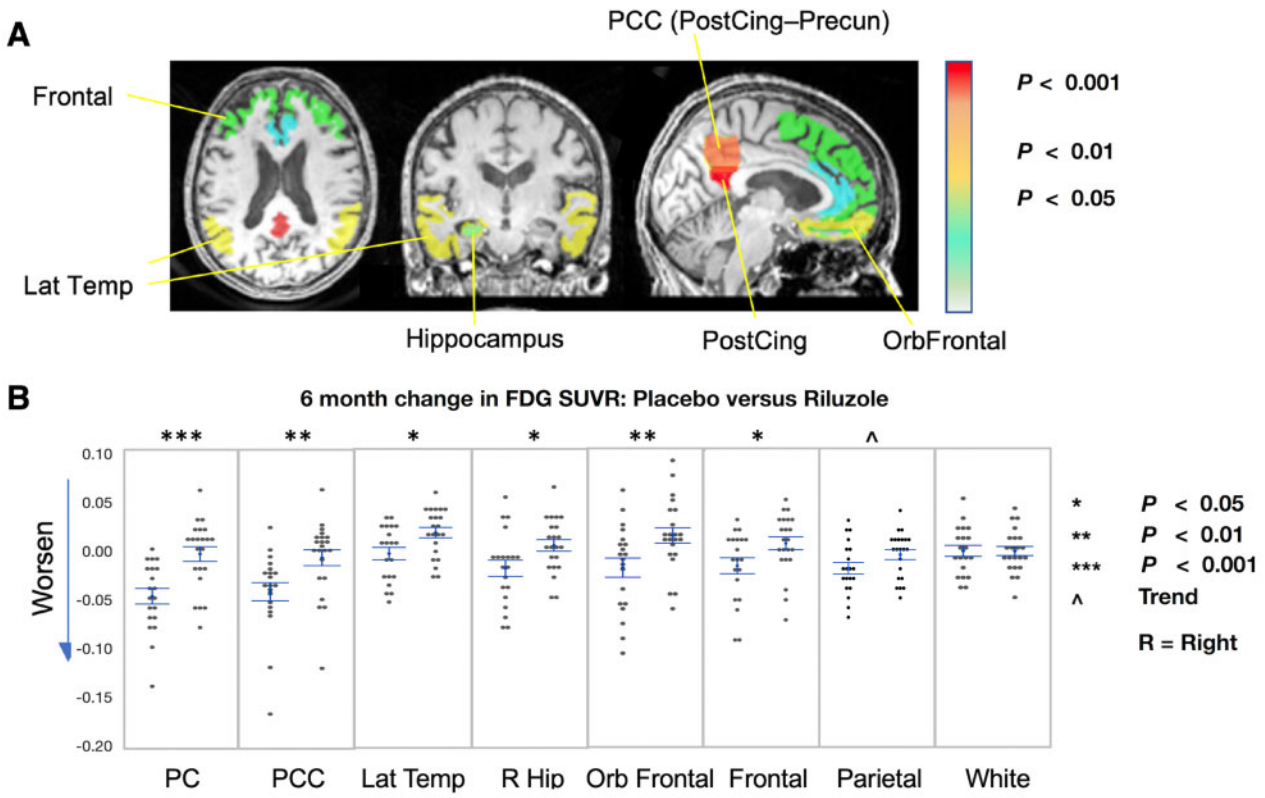

Figure 4 Comparison of changes in FDG-PET in prespecified regions of interest over 6 months. (**A**) Region of interest boundaries shown in representative slices, colour-coded to indicate the significance levels in comparisons between placebo and riluzole-treated arms of the 6 month change in FDG SUVR. (**B**) Comparison between placebo and riluzole-treated arms of the 6 month change in FDG SUVR for posterior cingulate (PC = PostCing), combined PC and precuneus (PCC), lateral temporal (LatTemp), right hippocampus (Hip), orbitofrontal (OrbFrontal), frontal, parietal and subcortical white matter (as a comparator, expected to remain stable). For each region, data-points are shown for the placebo group on the *left* and for the riluzole-treated group on the *right*. Individual values are shown with mean and standard error bars.

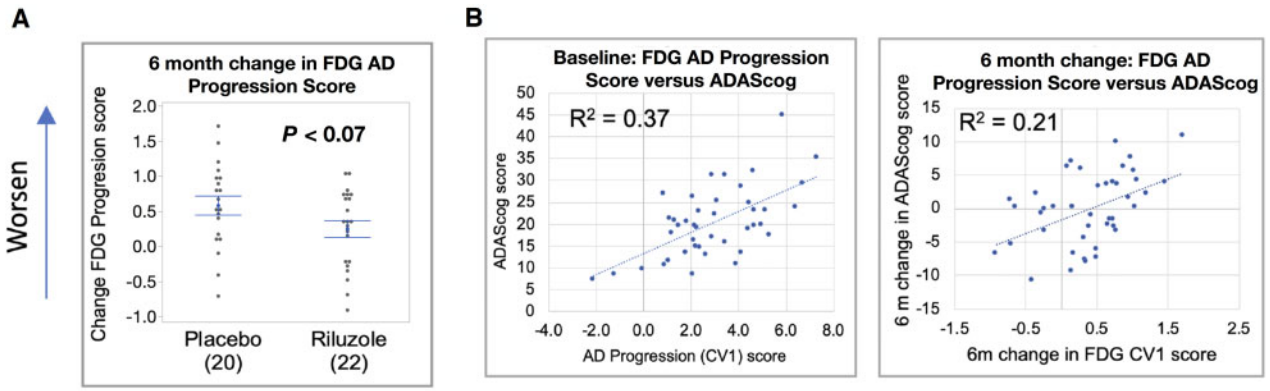

Figure 5 Comparison of FDG-PET progression score changes over 6 months. (**A**) Comparison between placebo and riluzole-treated arms of the change in FDG progression score. (**B**) Correlation between Alzheimer's disease progression score at baseline and ADAS-cog score at baseline (*left*) and between the 6-month change in Alzheimer's disease progression score and in ADAS-cog (*right*) for all study participants.

were also observed in precuneus, lateral temporal cortex, right hippocampus and frontal cortex. Glutamate levels measures with ^{1}H MRS, a secondary outcome, showed a significant or trend-level group × visit interaction in PC, whereby the levels of this excitatory amino acid neurotransmitter increased after three months of treatment, suggesting the possibility that riluzole engages the glutamatergic system as its therapeutic target. No changes were found in the ^{1}H MRS levels of NAA, our second primary outcome measure. A significant correlation was observed between cognitive measures and cerebral metabolism in FDG-PET, a key measure of brain function in Alzheimer's disease. PC glutamate levels also correlated with cognitive performance. Our study provides the first in-human data supporting a potential therapeutic benefit of riluzole in patients with Alzheimer's disease.

The beneficial effects of riluzole on neuronal function and cognition observed in this pilot study could be attributable to one or more of the mechanisms that have been established in rodent models. In this mild Alzheimer's disease population, where

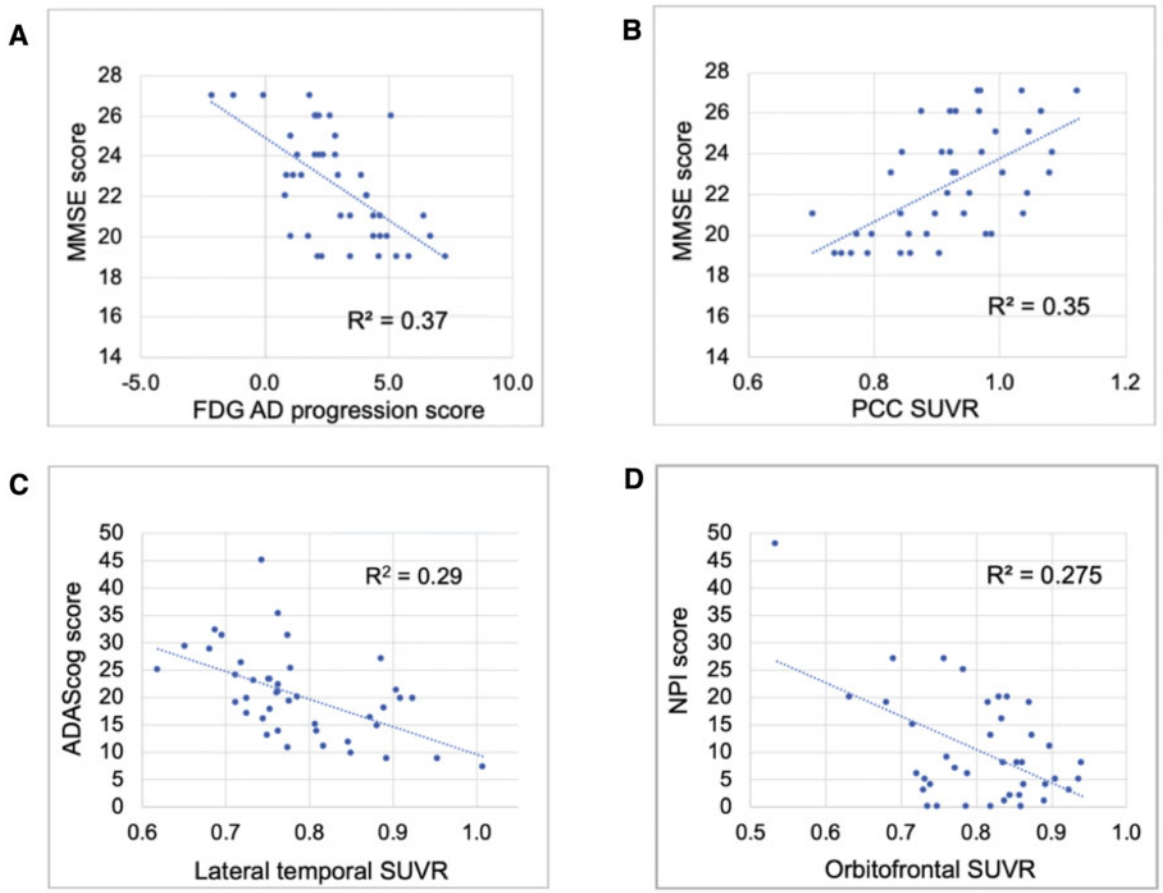

Figure 6 Correlations between FDG-PET measures and cognitive performance. Correlations at baseline between: (**A**) FDG Alzheimer's disease progression score and MMSE score; (**B**) posterior cingulate-precuneus (PCC) score and MMSE score; (**C**) lateral temporal FDG SUVR and ADAS-cog score; and (**D**) orbitofrontal FDG SUVR and NPI score.

amyloid and tau were already well-established, the most likely mechanisms of therapeutic effect by riluzole could have been in preventing further damage to vulnerable pyramidal neurons through modulation of glutamate levels, reduced glutamate-mediated toxicity and increased synaptic activity. The directional favourable cognitive effects are consistent with the prevention of age-related cognitive decline found in rodent models.[22,26]

Similar effects on glucose metabolism were observed with riluzole as those reported for memantine in patients with Alzheimer's disease over the same time period,[65] with both studies finding greatest effects in PC and precuneus. Memantine acts on the glutamatergic system through NMDA receptor partial antagonism, reducing calcium ion influx and related toxicity.[66] Riluzole has shown similar mitigating effects on sodium and calcium ion influx, through protein kinase C (PKC) inhibition or by regulating glutamate transporter and modulation of ion channels leading to potential decreased glutamate overflow to extrasynaptic space rather than direct NMDA interaction.[67] Given memantine's effects on glucose metabolism, this mitigation may also have contributed to the effects of riluzole. The numerous effects of riluzole demonstrated preclinically may support additional therapeutic benefit in Alzheimer's disease.

FDG-PET was chosen as the main primary outcome measure in this study because it is a well-established biomarker of neuronal function in Alzheimer's disease,[64,68] and progressive hypometabolism in Alzheimer's disease-relevant regions strongly correlates with clinical progression.[62–64] The PC, in which the most robust treatment effect was observed in this study (Fig. 3A–C), is a hub network region and one of the earliest and most strongly affected regions in Alzheimer's disease.[69,70] The slower decline in cerebral glucose metabolism with riluzole was observed in both younger and older groups, males and females, and *APOE* ε4 carriers and non-carriers (Fig. 3D).

The observed lessening of metabolic decline in the riluzole group compared to placebo in several Alzheimer's disease-related regions of interest (Fig. 4) suggested an effect in Alzheimer's disease-related networks. Consistent with this, the Alzheimer's disease Progression Classifier score, previously validated in ADNI participants,[51] showed a trend-level slower disease progression in the riluzole-treated group than in the placebo group (Fig. 5A). This preservation supports further exploration of the apparent disease-modifying effect of riluzole in larger, longer, full-efficacy clinical trials, with assessments of clinical and neuroimaging changes at multiple time points to map the trajectory of therapeutic response. The less robust though significant effects in the Alzheimer's disease-related regions other than PC and precuneus may reflect technical factors including greater variability due to rotational head motion and differences in slice location from the reference region.

The trend-level differences in longitudinal Alzheimer's disease progression pattern expression between *APOE* ε4 carriers and non-carriers merits further study. A potential explanation may be due to baseline neural hyperexcitability in *APOE* ε4 carriers[71,72] that could be more responsive to glutamatergic modulation. It would be of interest to characterize patients with Alzheimer's disease for analysis stratification, as the population is highly heterogeneous

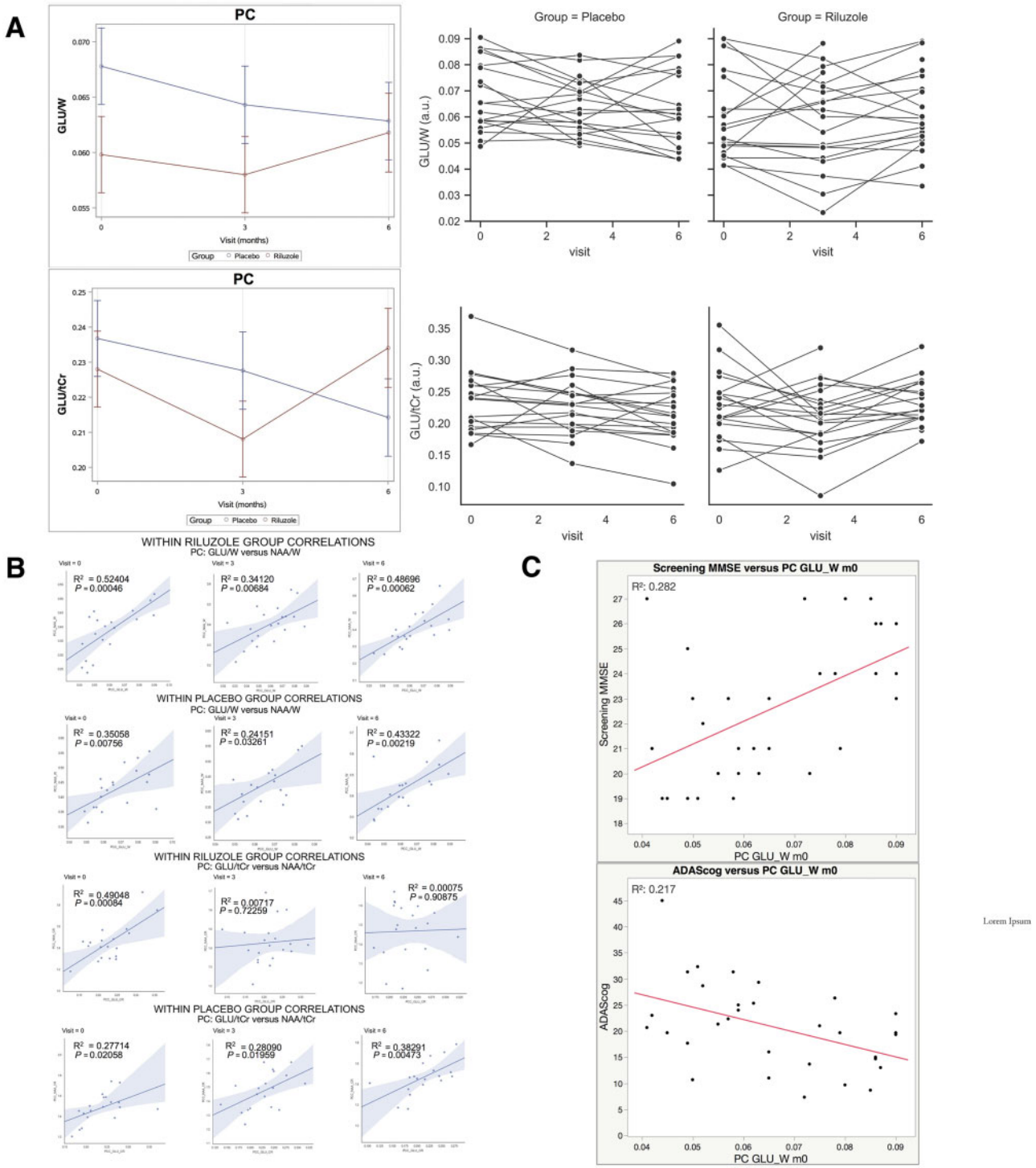

Figure 7 Comparison of changes in ^{1}H MRS measures. (**A**) ^{1}H MRS measures of Glu/W (*top*) and Glu/tCr (*bottom*) levels changes in PC at baseline, 3 and 6 months. (**B**) Correlations at baseline, midpoint and end point between NAA/W and Glu/W in riluzole and placebo groups (*top*) and NAA/tCr and Glu/tCr in riluzole and placebo groups (*bottom*). (**C**) Correlations at baseline between Glu/W and MMSE (*top*) and Glu/W and ADAS-cog (*bottom*) across participants.

with regard to clinical manifestations, rate of disease progression, tau burden, comorbidities and possibly treatment response. This heterogeneity was present in our study.

We observed a strong correlation between the FDG-PET Alzheimer's disease Progression Classifier score and ADAS-cog at baseline and in treatment change from baseline to 6 months (Fig. 5B). This is consistent with previous findings in the ADNI and other populations,[51] and suggests that FDG-PET progression scores are predictive of and aligned with cognitive changes. Examining placebo and riluzole groups separately, correlations at baseline were significant for both groups. Additional associations between FDG-PET glucose metabolism and cognitive measures at baseline were observed (Fig. 6). Use of biomarkers to predict cognitive effects in smaller trials could potentially lower clinical trial costs and play an important role in identifying which therapies should be advanced to larger trials.

^{1}H MRS has shown metabolic differences in Alzheimer's disease compared to matched normal individuals[73]; however, the results have not been sufficiently consistent to enable their use as reliable outcome measures in Alzheimer's disease in a manner analogous to FDG-PET measures of cerebral glucose metabolism. For example, in a study of memantine that showed no MRS effects despite favourable glucose metabolism effects, the authors noted that MRS results were affected by variability and patient-induced artefacts.[74] With riluzole an established glutamate modulator, this study sought to derive objective evidence of riluzole treatment target engagement by using ^{1}H MRS as a secondary outcome measure to measure in vivo brain levels of glutamatergic compounds. Our finding of a significant or trend-level group × visit interaction for PC glutamate, with its levels rising between 3 and 6 months of treatment (Fig. 7A) suggest potential engagement of the glutamatergic system by riluzole. This interpretion should be made with caution as it is a significance in a group × visit interaction and preliminary while there were no significant differences between groups from baseline to 6 months as originally hypothesized. It has been proposed that enhancing the efficiency of glutamatergic synaptic activity, which riluzole is postulated to accomplish, leads to an increase in intracellular glutamate levels,[75] which was probably the major contributor to the detected ^{1}H MRS glutamate signal. We sought to assess the effects of riluzole on neuronal viability and function through simultaneous ^{1}H MRS measurement of the putative neuronal marker NAA, but did not detect changes in NAA. Negative findings have also been reported in previous longitudinal ^{1}H MRS studies of Alzheimer's disease and ALS, which revealed cross-sectional but not longitudinal NAA changes, and attributed this to inter-participant variability and technical factors.[76,77] Depleted ^{1}H MRS levels of NAA and glutamate have been reported in Alzheimer's disease compared to healthy controls,[73,78,79] which could not be assessed in this study due to the lack of a normal comparison group. We observed an exploratory correlation between glutamate levels and cognitive measures in PC such as MMSE and ADAS-cog (Fig. 7C), with higher ^{1}H MRS glutamate levels associating positively with higher cognitive performance. The positive correlation between NAA and glutamate levels (Fig. 7B) was consistent with previous reports in the normal brain,[80] potentially underpinned by tight coupling of the two compounds in NAA synthesis in neuronal mitochondria by addition of glutamate-derived aspartate to an acetyl group derived from acetyl-CoA, in a reaction catalysed by L-aspartate-*N*-acetyltransferase.[81] Conversely, NAA has been postulated to serve as a reservoir of glutamate synthesis.[82] As an exploratory analysis, we observed a significant or trend group × visit interaction with increased GABA levels in left hippocampus with riluzole treatment. GABA is reportedly depleted in Alzheimer's disease and mild cognitive impairment.[83,84] Treatment-related increases in GABA levels (Supplementary Fig. 2B) suggest that riluzole may at least partially alleviate this reported deficit, with possible benefit given the positive correlation of GABA with memory performance in this study (Supplementary Fig. 2C). There was general agreement between the ratios of metabolite level peak ratios relative to unsuppressed water (W) and tCr in our study, but greater consistency in ratios measured relative to W. Caution has been urged in interpreting ratios relative to tCr because levels have been reported to change in a number of neuropsychiatric[85] and neurological disorders.[86] We provided both ratios for comparison with literature.

Riluzole was generally well tolerated, with no significant difference in side effects compared to placebo. Riluzole has been used for decades in the treatment of ALS. However, larger, longer duration studies are necessary to have a comprehensive evaluation of safety and efficacy of riluzole in the Alzheimer's disease population, and should precede its use in Alzheimer's disease outside of a monitored clinical trial.

This study has several limitations. First, the sample size was relatively small, and results require replication in larger-sample studies. A second limitation was the lack of amyloid characterization. However, the presence of an FDG-PET Alzheimer's disease pattern helped to confirm clinical diagnosis and has been shown to have a high degree of agreement with the presence of tau pathology.[87] Third, ^{1}H MRS is unable to differentiate neurotransmitter or vesicular and metabolic pools of glutamate or GABA, limiting interpretation. ^{1}H MRS data acquisition techniques require relatively large voxels for reliable quantification of metabolites, potentially leading to partial volume effects and masking of group effects. As noted in other studies, longitudinal MRS measurements can be subject to technical variability and participant head motion. The study was not powered for neuropsychological outcome measurement, and clinical changes must be viewed only as directional and exploratory.

In conclusion, a slower decline in cerebral glucose metabolism was observed in riluzole-treated patients with Alzheimer's disease than in placebo in multiple Alzheimer's disease-relevant brain regions, which correlated with cognitive performance. These findings support future fully powered clinical trials to further evaluate riluzole as a potential pharmacological therapy for Alzheimer's disease.

Acknowledgements

We thank the patients and their families for their collaboration and help in this study. We thank Dr Sam Gandy for recruitment support and Gargi Padki for research coordination support. We thank Muc Chieu Du, Simon Morim and Jojo Borja for their work in image data acquisition, and Laura Matthews for her assistance in preliminary analyses of the FDG-PET data. We also thank Drs Barbara O'Sullivan and Judith Neugroschl for blood test results revision.

Funding

This trial was funded by Alzheimer's Drug Discovery Foundation and Dana Foundation (A.C.P.) with support from Mount Sinai Alzheimer's Disease Research Center P30AG066514 and P50AG05138-20, The Rockefeller University grant number UL1 TR001866 from the National Center for Advancing Translational Sciences (NCATS), National Institutes of Health (NIH) Clinical and Translational Science Award (CTSA) program. A.C.P. is also funded by NIH R01 AG063819, NIH R01AG064020, Paul B. Beeson Emerging Leaders Career Development Award in Ageing K76 AG054772, the BrightFocus Foundation, the DANA Foundation, the Alzheimer's Drug Discovery Foundation, the Alzheimer's Association, the Robert J. and Claire Pasarow Foundation, the Carolyn and Eugene Mercy Research Support, the Bernard L. Schwartz Award for Physician Scientist and the Karen Strauss Cook Research Scholar Award. D.C.S. received support from 1 R01 MH075895.

Competing interests

A.C.P. has patent applications 17/026,181 and PCT/2021/053403 related to riluzole. Rockefeller University through grant from the Alzheimer's Drug Discovery Foundation (ADDF) provided funds to ADM Diagnostics to D.C.M. for FDG-PET analysis. Icahn School of Medicine at Mount Sinai through ADDF grant provided funds to XsOsNMR consulting to D.C.S. for ^{1}H MRS analysis.

Supplementary material

Supplementary material is available at *Brain* online.

References

1. 2020 Alzheimer's disease facts and figures. *Alzheimers Dement*. Published online 10 March 2020. 10.1002/alz.12068
2. Morrison JH, Hof PR. Life and death of neurons in the aging brain. *Science*. 1997;278(5337):412–419.
3. Morrison JH, Hof PR. Selective vulnerability of corticocortical and hippocampal circuits in aging and Alzheimer's disease. *Prog Brain Res*. 2002;136:467–486.
4. Crimins JL, Pooler A, Polydoro M, Luebke JI, Spires-Jones TL. The intersection of amyloid beta and tau in glutamatergic synaptic dysfunction and collapse in Alzheimer's disease. *Ageing Res Rev*. 2013;12(3):757–763.
5. Hof PR, Morrison JH. Quantitative analysis of a vulnerable subset of pyramidal neurons in Alzheimer's disease: II. Primary and secondary visual cortex. *J Comp Neurol*. 1990;301(1):55–64.
6. Hof PR, Cox K, Morrison JH. Quantitative analysis of a vulnerable subset of pyramidal neurons in Alzheimer's disease: I. Superior frontal and inferior temporal cortex. *J Comp Neurol*. 1990;301(1):44–54.
7. Hardingham GE, Bading H. Synaptic versus extrasynaptic NMDA receptor signalling: Implications for neurodegenerative disorders. Nat Rev Neurosci. 2010;11(10):682–696.
8. Hardingham GE, Fukunaga Y, Bading H. Extrasynaptic NMDARs oppose synaptic NMDARs by triggering CREB shut-off and cell death pathways. *Nat Neurosci*. 2002;5(5):405–414.
9. Sharma A, Kazim SF, Larson CS, et al. Divergent roles of astrocytic versus neuronal EAAT2 deficiency on cognition and overlap with aging and Alzheimer's molecular signatures. *Proc Natl Acad Sci U S A*. 2019;116(43):21800–21811.
10. Braak H, Del Tredici K. Spreading of tau pathology in sporadic Alzheimer's disease along cortico-cortical top-down connections. *Cereb Cortex*. 2018;28(9):3372–3384.
11. Morrison JH, Hof PR. Life and death of neurons in the aging cerebral cortex. *Intl Rev Neurobiol*. 2007;81:41–57.
12. Hof PR, Morrison JH. Neocortical neuronal subpopulations labeled by a monoclonal antibody to calbindin exhibit differential vulnerability in Alzheimer's disease. *Exp Neurol*. 1991;111(3):293–301.
13. Esclaire F, Lesort M, Blanchard C, Hugon J. Glutamate toxicity enhances tau gene expression in neuronal cultures. *J Neurosci Res*. 1997;49(3):309–318.
14. Sindou P, Lesort M, Couratier P, Yardin C, Esclaire F, Hugon J. Glutamate increases tau phosphorylation in primary neuronal cultures from fetal rat cerebral cortex. *Brain Res*. 1994;646(1):124–128.
15. Pooler AM, Phillips EC, Lau DH, Noble W, Hanger DP. Physiological release of endogenous tau is stimulated by neuronal activity. *EMBO Rep*. 2013;14(4):389–394.
16. Yamada K, Holth JK, Liao F, et al. Neuronal activity regulates extracellular tau in vivo. *J Exp Med*. 2014;211(3):387–393.
17. Wu JW, Hussaini SA, Bastille IM, et al. Neuronal activity enhances tau propagation and tau pathology in vivo. *Nat Neurosci*. 2016;19(8):1085–1092.
18. Li S, Hong S, Shepardson NE, Walsh DM, Shankar GM, Selkoe D. Soluble oligomers of amyloid Beta protein facilitate hippocampal long-term depression by disrupting neuronal glutamate uptake. *Neuron*. 2009;62(6):788–801.
19. Li S, Jin M, Koeglsperger T, Shepardson NE, Shankar GM, Selkoe DJ. Soluble Abeta oligomers inhibit long-term potentiation through a mechanism involving excessive activation of extrasynaptic NR2B-containing NMDA receptors. *J Neurosci*. 2011;31(18):6627–6638.
20. Kamenetz F, Tomita T, Hsieh H, et al. APP processing and synaptic function. *Neuron*. 2003;37(6):925–937.
21. Snyder EM, Nong Y, Almeida CG, et al. Regulation of NMDA receptor trafficking by amyloid-beta. *Nature Neurosci*. 2005;8(8):1051–1058.
22. Pereira AC, Lambert HK, Grossman YS, et al. Glutamatergic regulation prevents hippocampal-dependent age-related cognitive decline through dendritic spine clustering. *Proc Natl Acad Sci U S A*. 2014;111(52):18733–18738.
23. Govindarajan A, Kelleher RJ, Tonegawa S. A clustered plasticity model of long-term memory engrams. *Nat Rev Neurosci*. 2006;7(7):575–583.
24. Larkum ME, Nevian T. Synaptic clustering by dendritic signalling mechanisms. *Curr Opin Neurobiol*. 2008;18(3):321–331.
25. Pereira AC, Gray JD, Kogan JF, et al. Age and Alzheimer's disease gene expression profiles reversed by the glutamate modulator riluzole. *Mol Psychiatry*. 2016;22(2):296–305.
26. Okamoto M, Gray JD, Larson CS, et al. Riluzole reduces amyloid beta pathology, improves memory, and restores gene expression changes in a transgenic mouse model of early-onset Alzheimer's disease. *Transl Psychiatry*. 2018;8(1):153.
27. Colonna M, Wang Y. TREM2 variants: New keys to decipher Alzheimer disease pathogenesis. *Nat Rev Neurosci*. 2016;17(4):201–207.
28. Streit WJ. Microglia and Alzheimer's disease pathogenesis. *J Neurosci Res*. 2004;77(1):1–8.
29. Butovsky O, Jedrychowski MP, Moore CS, et al. Identification of a unique TGF-beta-dependent molecular and functional signature in microglia. *Nat Neurosci*. 2014;17(1):131–143.
30. Keren-Shaul H, Spinrad A, Weiner A, et al. A unique microglia type associated with restricting development of Alzheimer's disease. *Cell*. 2017;169(7):1276–1290.e17.
31. Hunsberger HC, Weitzner DS, Rudy CC, et al. Riluzole rescues glutamate alterations, cognitive deficits, and tau pathology associated with P301L tau expression. *J Neurochem*. 2015;135(2):381–394.
32. Pontecorvo MJ, Devous MD, Kennedy I, et al. A multicentre longitudinal study of flortaucipir (18F) in normal ageing, mild cognitive impairment and Alzheimer's disease dementia. *Brain*. 2019;142(6):1723–1735.
33. Cao YJ, Dreixler JC, Couey JJ, Houamed KM. Modulation of recombinant and native neuronal SK channels by the neuroprotective drug riluzole. *Eur J Pharmacol*. 2002;449(1-2):47–54.
34. Urbani A, Belluzzi O. Riluzole inhibits the persistent sodium current in mammalian CNS neurons. *Eur J Neurosci*. 2000;12(10):3567–3574.
35. Katoh-Semba R, Asano T, Ueda H, et al. Riluzole enhances expression of brain-derived neurotrophic factor with consequent proliferation of granule precursor cells in the rat hippocampus. *Faseb J*. 2002;16(10):1328–1330.
36. Mizuta I, Ohta M, Ohta K, Nishimura M, Mizuta E, Kuno S. Riluzole stimulates nerve growth factor, brain-derived neurotrophic factor and glial cell line-derived neurotrophic factor synthesis in cultured mouse astrocytes. *Neurosci Lett*. 2001;310(2-3):117–120.
37. Chowdhury GM, Banasr M, de Graaf RA, Rothman DL, Behar KL, Sanacora G. Chronic riluzole treatment increases glucose metabolism in rat prefrontal cortex and hippocampus. *J Cerebral Blood Flow Metabol*. 2008;28(12):1892–1897.
38. Banasr M, Chowdhury GM, Terwilliger R, et al. Glial pathology in an animal model of depression: Reversal of stress-induced cellular, metabolic and behavioral deficits by the glutamate-modulating drug riluzole. *Mol Psychiatry*. 2010;15(5):501–511.
39. Fumagalli E, Funicello M, Rauen T, Gobbi M, Mennini T. Riluzole enhances the activity of glutamate transporters GLAST, GLT1 and EAAC1. *Eur J Pharmacol*. 2008;578(2-3):171–176.

40. Frizzo ME, Dall'Onder LP, Dalcin KB, Souza DO. Riluzole enhances glutamate uptake in rat astrocyte cultures. *Cell Mol Neurobiol*. 2004;24(1):123–128.
41. Sibson NR, Dhankhar A, Mason GF, Rothman DL, Behar KL, Shulman RG. Stoichiometric coupling of brain glucose metabolism and glutamatergic neuronal activity. *Proc Natl Acad Sci U S A*. 1998;95(1):316–321.
42. Shen J, Petersen KF, Behar KL, et al. Determination of the rate of the glutamate/glutamine cycle in the human brain by in vivo 13C NMR. *Proc Natl Acad Sci U S A*. 1999;96(14):8235–8240.
43. Magistretti PJ. Role of glutamate in neuron-glia metabolic coupling. *Am J Clin Nutr*. 2009;90(3):875S–880S.
44. Patel AB, Lai JC, Chowdhury GM, et al. Direct evidence for activity-dependent glucose phosphorylation in neurons with implications for the astrocyte-to-neuron lactate shuttle. *Proc Natl Acad Sci U S A*. 2014;111(14):5385–5390.
45. McKhann G, Drachman D, Folstein M, Katzman R, Price D, Stadlan EM. Clinical diagnosis of Alzheimer's disease: Report of the NINCDS-ADRDA Work Group under the auspices of Department of Health and Human Services Task Force on Alzheimer's Disease. Guideline Practice Guideline. *Neurology*. 1984;34(7):939–944.
46. McKhann GM, Knopman DS, Chertkow H, et al. The diagnosis of dementia due to Alzheimer's disease: Recommendations from the National Institute on Aging-Alzheimer's Association workgroups on diagnostic guidelines for Alzheimer's disease. *Alzheimer's Dement*. 2011;7(3):263–269.
47. Rosen WG, Mohs RC, Davis KL. A new rating scale for Alzheimer's disease. *Am J Psychiatry*. 1984;141(11):1356–1364.
48. Mohs RC, Knopman D, Petersen RC, et al. Development of cognitive instruments for use in clinical trials of antidementia drugs: Additions to the Alzheimer's Disease Assessment Scale that broaden its scope. The Alzheimer's Disease Cooperative Study. *Alzheimer Dis Assoc Disord*. 1997;11(Suppl 2):S13–21.
49. Galasko D, Bennett D, Sano M, et al. An inventory to assess activities of daily living for clinical trials in Alzheimer's disease. The Alzheimer's Disease Cooperative Study. *Alzheimer Dis Assoc Disord*. 1997;11(Suppl 2):S33–9.
50. Cummings JL, Mega M, Gray K, Rosenberg-Thompson S, Carusi DA, Gornbein J. The Neuropsychiatric Inventory: Comprehensive assessment of psychopathology in dementia. *Neurology*. 1994;44(12):2308–2314.
51. Matthews DC, Lukic AS, Andrews RD, et al. Dissociation of Down syndrome and Alzheimer's disease effects with imaging. *Alzheimers Dement (N Y)*. 2016;2(2):69–81.
52. Peters F, Perani D, Herholz K, et al. Orbitofrontal dysfunction related to both apathy and disinhibition in frontotemporal dementia. *Dement Geriatr Cogn Disord*. 2006;21(5-6):373–379.
53. Mega MS, Dinov ID, Porter V, et al. Metabolic patterns associated with the clinical response to galantamine therapy: A fludeoxyglucose f 18 positron emission tomographic study. *Arch Neurol*. 2005;62(5):721–728.
54. Maass A, Landau S, Baker SL, et al. Comparison of multiple tau-PET measures as biomarkers in aging and Alzheimer's disease. *Neuroimage*. 2017;157:448–463.
55. Fischl B, Salat DH, Busa E, et al. Whole brain segmentation: Automated labeling of neuroanatomical structures in the human brain. *Neuron*. 2002;33(3):341–355.
56. Tzourio-Mazoyer N, Landeau B, Papathanassiou D, et al. Automated anatomical labeling of activations in SPM using a macroscopic anatomical parcellation of the MNI MRI single-subject brain. *Neuroimage*. 2002;15(1):273–289.
57. Romano S, Coarelli G, Marcotulli C, et al. Riluzole in patients with hereditary cerebellar ataxia: A randomised, double-blind, placebo-controlled trial. *Lancet Neurol*. 2015;14(10):985–991.
58. Dreher W, Leibfritz D. Detection of homonuclear decoupled in vivo proton NMR spectra using constant time chemical shift encoding: CT-PRESS. *Magn Reson Imaging*. 1999;17(1):141–150.
59. Mayer D, Spielman DM. Detection of glutamate in the human brain at 3 T using optimized constant time point resolved spectroscopy. *Magn Reson Med* 2005;54(2):439–442.
60. Girgis RR, Baker S, Mao X, et al. Effects of acute *N*-acetylcysteine challenge on cortical glutathione and glutamate in schizophrenia: A pilot in vivo proton magnetic resonance spectroscopy study. *Psychiatry Res*. 2019;275:78–85.
61. Shungu DC, Mao X, Gonzales R, et al. Brain gamma-aminobutyric acid (GABA) detection in vivo with the J-editing (1) H MRS technique: A comprehensive methodological evaluation of sensitivity enhancement, macromolecule contamination and test-retest reliability. *NMR Biomed*. 2016;29(7):932–942.
62. Landau SM, Harvey D, Madison CM, et al.; Alzheimer's Disease Neuroimaging Initiative. Associations between cognitive, functional, and FDG-PET measures of decline in Alzheimer's disease and MCI. *Neurobiol Aging*. 2011;32(7):1207–1218.
63. Khosravi M, Peter J, Wintering NA, et al. 18F-FDG is a superior indicator of cognitive performance compared to 18F-Florbetapir in Alzheimer's Disease and mild cognitive impairment evaluation: A global quantitative analysis. *J Alzheimers Dis*. 2019;70(4):1197–1207.
64. Alexander GE, Chen K, Pietrini P, Rapoport SI, Reiman EM. Longitudinal PET evaluation of cerebral metabolic decline in Dementia: A potential outcome measure in Alzheimer's disease treatment studies. *Am J Psychiatry*. 2002;159(5):738–745.
65. Wang T, Huang Q, Reiman EM, et al. Effects of memantine on clinical ratings, fluorodeoxyglucose positron emission tomography measurements, and cerebrospinal fluid assays in patients with moderate to severe Alzheimer dementia: A 24-week, randomized, clinical trial. *J Clin Psychopharmacol*. 2013;33(5):636–642.
66. Revett TJ, Baker GB, Jhamandas J, Kar S. Glutamate system, amyloid ss peptides and tau protein: Functional interrelationships and relevance to Alzheimer disease pathology. *J Psychiatry Neurosci*. 2013;38(1):6–23.
67. Lipton SA. The molecular basis of memantine action in Alzheimer's disease and other neurologic disorders: Low-affinity, uncompetitive antagonism. *Curr Alzheimer Res*. 2005;2(2):155–165.
68. Mosconi L, Tsui WH, Herholz K, et al. Multicenter standardized 18F-FDG PET diagnosis of mild cognitive impairment, Alzheimer's disease, and other dementias. *J Nucl Med*. 2008;49(3):390–398.
69. Minoshima S, Giordani B, Berent S, Frey KA, Foster NL, Kuhl DE. Metabolic reduction in the posterior cingulate cortex in very early Alzheimer's disease. *Ann Neurol*. 1997;42(1):85–94.
70. Mutlu J, Landeau B, Tomadesso C, et al. Connectivity disruption, atrophy, and hypometabolism within posterior cingulate networks in Alzheimer's disease. *Front Neurosci*. 2016;10:582.
71. Koelewijn L, Lancaster TM, Linden D, et al. Oscillatory hyperactivity and hyperconnectivity in young APOE-ε4 carriers and hypoconnectivity in Alzheimer's disease. *eLife*. 2019;8:e36011.
72. Nuriel T, Angulo SL, Khan U, et al. Neuronal hyperactivity due to loss of inhibitory tone in APOE4 mice lacking Alzheimer's disease-like pathology. *Nat Commun*. 2017;8(1):1464.
73. Graff-Radford J, Kantarci K. Magnetic resonance spectroscopy in Alzheimer's disease. *Neuropsychiatr Dis Treat*. 2013;9:687–696.
74. Schmidt R, Ropele S, Pendl B, et al. Longitudinal multimodal imaging in mild to moderate Alzheimer disease: A pilot study with memantine. *J Neurol Neurosurg Psychiatry*. 2008;79(12):1312–1317.
75. Penner J, Rupsingh R, Smith M, Wells JL, Borrie MJ, Bartha R. Increased glutamate in the hippocampus after galantamine treatment for Alzheimer disease. *Prog Neuropsychopharmacol Biol Psychiatry*. 2010;34(1):104–110.

76. Kalra S. Magnetic resonance spectroscopy in ALS. *Front Neurol*. 2019;10:482.
77. Schott JM, Frost C, MacManus DG, Ibrahim F, Waldman Alzheimer's disease, Fox NC. Short echo time proton magnetic resonance spectroscopy in Alzheimer's disease: A longitudinal multiple time point study. *Brain*. 2010;133(11):3315–3322.
78. Fayed N, Modrego PJ, Rojas-Salinas G, Aguilar K. Brain glutamate levels are decreased in Alzheimer's disease: A magnetic resonance spectroscopy study. *Am J Alzheimer's Dis Other Demen*. 2011;26(6): 450–456.
79. Hattori N, Abe K, Sakoda S, Sawada T. Proton MR spectroscopic study at 3 Tesla on glutamate/glutamine in Alzheimer's disease. *Neuroreport*. 2002;13(1):183–186.
80. Kraguljac NV, Reid MA, White DM, den Hollander J, Lahti AC. Regional decoupling of N-acetyl-aspartate and glutamate in schizophrenia. *Neuropsychopharmacology*. 2012;37(12):2635–2642.
81. Birken DL, Oldendorf WH. N-acetyl-L-aspartic acid: A literature review of a compound prominent in 1H-NMR spectroscopic studies of brain. *Neurosci Biobehav Rev*. 1989; 13(1):23–31.
82. Clark JF, Doepke A, Filosa JA, et al. N-acetylaspartate as a reservoir for glutamate. *Med Hypotheses*. 2006;67(3):506–512.
83. Gueli MC, Taibi G. Alzheimer's disease: Amino acid levels and brain metabolic status. *Neurol Sci*. 2013;34(9):1575–1579.
84. Bai X, Edden RA, Gao F, et al. Decreased gamma-aminobutyric acid levels in the parietal region of patients with Alzheimer's disease. *J Magn Reson Imaging*. 2015;41(5):1326–1331.
85. Ongur D, Prescot AP, Jensen JE, Cohen BM, Renshaw PF. Creatine abnormalities in schizophrenia and bipolar disorder. *Psychiatry Res*. 2009;172(1):44–48.
86. Weiduschat N, Mao X, Hupf J, et al. Motor cortex glutathione deficit in ALS measured in vivo with the J-editing technique. *Neurosci Lett*. 2014;570:102–107.
87. Matthews DC, Ritter A, Thomas RG, et al. Rasagiline effects on glucose metabolism, cognition, and tau in Alzheimer's dementia. *Alzheimers Dement (N Y)*. 2021;7(1):e12106.